Congresso de Métodos Numéricos em Engenharia 2015
Lisboa, 29 de Junho a 2 de Julho 2015

EFFICIENT SIMULATION OF THE EFFECTIVE G-FACTOR FOR CARRIERS CONFINED IN SEMICONDUCTOR NANO-OBJECTS

Li-Wei Yang[1], Chin-Min Yang[2], Yiming Li[2], and Oleksandr Voskoboynikov[1*]

1: Department of Electronics Engineering
National Chiao Tung University
1001 Ta Hsueh Rd. Hsinchu 30010, Taiwan
e-mail: wayne_yang24@hotmail.com
*e-mail: vam@faculty.nctu.edu.tw
2: Department of Electrical and Computer Engineering
National Chiao Tung University
1001 Ta Hsueh Rd. Hsinchu 30010, Taiwan
e-mail: cmyang@mail.ymlab.org
e-mail: ymli@mail.ymlab.org

Keywords: Semiconductor, Quantum Dot, Spin-Orbit Interaction, G-factor

Abstract. *In this paper we present an efficient method of the full three-dimensional simulation of the effective g-factor tensor for electrons in semiconductor nano-objects of complex geometry and material content. Taking the spin-orbit interaction, lattice strain, and external electric field into account, we numerically study the effective electron g-factor tensor for InAs/GaAs lateral asymmetrical quantum dot molecules, as an example. Our calculation method allows us very cost-effectively to simulate the effective g-factor properties within a wide range of the system parameters' changes when the Rashba and Dresselhaus spin-orbit couplings are considered. We demonstrate that the components, and three-dimensional anisotropy of the effective g-factor tensor can be controlled statically (in-situ configuration of the quantum molecule geometrical parameters) and dynamically (by application of the external electric field). We have obtained the components of the electron g-factor tensor and the factor anisotropy ratio in good agreement with the experimental observations. Our computational approach can be applied for the realistic modeling of selective manipulations of isolated and entangled spins in semiconductor nano-objects of complex geometry and material content.*

1 INTRODUCTION

Recent impressive development of semiconductor nano-technologies (lithography, colloidal chemistry, epitaxial growth, etc.) have made it possible to produce semiconductor nano-objects within a wide range of geometrical shapes and material parameters (among them

we can refer to self-assembled quantum dots, quantum rings, quantum dot molecules, quantum dot posts, nano-rods, nano-cubes, nano-wires, etc.), investigate their properties in details, and use them for various applications (see, for instance, [1][2][3][4][5] and references therein). Those semiconductor nano-objects are thought to be very promising candidates for practical use in optics, nano-biology, nano-medicine [6][7], and quantum information technology [8][9]

Nano-elements (nano-objects) which can be used in semiconductor-based quantum computation (or more wider – in semiconductor based spintronics) can provide us with universal control of the electron spins (see, for instance, [10][11][12] and references therein). Static and dynamic control of isolated spins in semiconductor nano-objects can be achieved through coupling electron (hole) momentum to the particle spins. Therefore, the spin-orbit coupling (interaction) offers desirable possibilities of the spin control in semiconductor nano-structures. For instance, a single electron spin control has been demonstrated recently in pure wurtzine $InAs$ nano-wire quantum dots due to the strong spin-orbit interaction (see, for instance, [13] and references therein). The spin-splitting of electrons or holes energy states in semiconductor nano-objects at non-zero magnetic field B is resulting in a finite Zeeman energy splitting ΔE and characterized by the effective Landé factor (g-factor) which can be defined as: $g = \Delta E/\mu_B B$ (μ_B is the Bohr magneton). Robust spin manipulations and spin-based qubit operations with an external electric/magnetic field in semiconductor nano-objects requires for proper (static and dynamic) techniques to control the particles' effective g-factors. Actually we can tune the effective magnetic (spin) response of the electrons confined in semiconductor nano-object (modifying the g-factor) by a proper structural engineering. Therefore, it is important to develop a microscopic understanding of the influence of the geometrical and material parameters of the nano-objects on the spin-orbit coupling and magnetic response of an individual carrier confined in the objects.

Recently the issue of the effective g-factor of electrons and holes confined in semiconductor self-assembled nano-structures (quantum dots and quantum dot molecules) was extensively studied both experimentally and theoretically. It was found that in general in low-dimensional semiconductor structures the effective g-factor becomes anisotropic and significantly depends on the direction of the magnetic field in the quantum structures. Therefore, it is represented as a tensor with components g_{ij}. The eight-band simulation of the effective g-factor in $InAs/GaAs$ lens shaped quantum dots predicted an increase of the absolute values of the electron and hole g-tensor diagonal components with increasing the dot size [14]. Simulated the electron and hole effective g-factor values and trends are substantially different from those seen in bulk semiconductors [15][16]. The anisotropy of the spin-splitting and g-factor of the electron ground states in $InAs$ quantum dots was found experimentally [17]. In agreement with theoretical predictions, the hole g-factor shows a much more pronounced anisotropy than that for the electrons [18]. The dynamic manipulation by external electric fields of the effective hole g-factor was demonstrated [19] by magneto-photoluminescence study of individual vertically stacked

$InAs/GaAs$ quantum dot molecules. The theory predicts the electric field tunable and asymmetric (because of the asymmetry in the spin-orbit coupling) electron g-factor for some geometries of self-assembled InAs/GaAs [20].

The interest to tune and manipulate of the electron effective g-factors in semiconductor quantum dots originates from a simple and pure spinor presentation for the conduction electron spin-states in semiconductors (unlike the hole spin-states). The presentation is demanded for the implementation of quantum bits in semiconductor nano-structures. As mentioned above, in general the anisotropy of the spin-orbit interaction leads to the anisotropic effective g-factor. The spin-orbit interaction in any forms is essentially three-dimensional (3D) because it is presented by three non-coplanar vectors: the effective built-in (or external) electric field, electron momentum operator, and vector of the Pauli (spin) matrices. Contrary to this fact, most of the one conduction band simulations use only the two-dimensional (2D) approximation ("adiabatic approximation", see for instance [21]) for the spin-orbit interaction (e.g. [22][23] and others). However, the adiabatic approximation is relevant to a proposition (postulate) that the inherently 3D problem can be presented by a coupled quasi-separable 1D+2D problem. At the same time, for relatively small nano-objects or nano-objects with rapid changes of their shape profiles the value of the accumulated error of this approximation cannot be clarified easily and it always requires for a special investigation [24]. That is why theoretical simulations based on this approximation can lead to some unphysical results. For instance, the 2D approximation obviously needs specified directions and magnitude of the effective (or external) electric field and cannot explain the built-in 3D anisotropy of the electron g-factor in semiconductor quantum dots. For the one conduction band approximation with the Rashba [25][26] and Dresselhaus [27] spin-orbit coupling models the use of the realistic full 3D description is prerequisite to any simulation of small nano-objects, nano-objects of complex shape and material content profiles, and combined nano-objects (molecules). The 2D based calculations for quantum dots [23][28][29] and quantum dot molecules [30],no matter how, should be confirmed by results obtained within the full 3D description [24]. In addition, the description should provide us with efficient tools for theoretical studies on the tuning and optimization of the anisotropic electron effective g-factors in highly asymmetrical semiconductor nano-objects with complex geometry [31][32].

In this paper, within the effective one electronic band approximation and including the Rashba and Dresselhaus spin-orbit interactions, we develop an efficient approach to the simulation of the effective g-factor for electrons confined in the semiconductor nano-objects with complex geometry and material content. We demonstrate the approach efficiency for the full 3D description of the electron g-factor anisotropy in lateral molecules combined from two semiconductor identical ("symmetric molecule") and not identical ("asymmetric molecule") lens shaped quantum dots. This makes it possible to investigate theoretically the important issue of the static (structural, material) and dynamic (induced by external fields) tuning of the effective g-factor. The results of this study clearly show that the proposed description and simulation data are appropriate for ex-

periments with molecules combined from two $InAs/GaAs$ small semiconductor quantum dots.

2 THEORETICAL MODEL AND METHOD OF SIMULATION

2.1 One electronic band effective Hamiltonian

We describe single electron energy states in III-V embedded (into the semiconductor matrix and combined into a lateral quantum dot molecule) semiconductor self-assembled quantum dots in the presence of the external magnetic $\mathbf{B}$ and electric $\mathbf{F}$ fields using the effective one electronic band energy (E) and position ($\mathbf{r}$) dependent Hamiltonian [33][34][35] which includes the spin-orbit interaction [25][26][27][36][37][38]:

$$\hat{\mathbf{H}} = \hat{\mathbf{H}}_e + \hat{\mathbf{H}}_{spin}, \tag{1}$$

where the spin-independent part is written as

$$\hat{\mathbf{H}}_e = \left[\hat{\mathbf{\Pi}}\frac{1}{2m\left(\mathbf{r},E\right)}\hat{\mathbf{\Pi}} - e\mathbf{F}\cdot\mathbf{r} + V(\mathbf{r})\right]\hat{\mathbf{I}}_2, \tag{2}$$

and

$$\hat{\mathbf{H}}_{spin} = \hat{\mathbf{H}}_M + \hat{\mathbf{H}}_R + \hat{\mathbf{H}}_D. \tag{3}$$

is the Hamiltonian which is relevant to the carrier's spin. In Eqs. (1)-(3) we define correspondingly

$$\hat{\mathbf{H}}_M = \frac{1}{2}\mu_B g_m\left(\mathbf{r},E\right)\hat{\sigma}\cdot\mathbf{B}, \tag{4}$$

$$\begin{aligned}\hat{\mathbf{H}}_R &= \left[\nabla_{\mathbf{r}}\beta\left(\mathbf{r},E\right) + \alpha\left(\mathbf{r},E\right)\mathbf{F}\right]\cdot\left[\hat{\sigma}\times\hat{\mathbf{\Pi}}\right] \\ &\equiv \mathbf{\Lambda}\left(\mathbf{r},E\right)\cdot\left[\hat{\sigma}\times\hat{\mathbf{\Pi}}\right],\end{aligned} \tag{5}$$

$$\hat{\mathbf{H}}_D = \gamma\left(\mathbf{r}\right)\sum_{\{i,j,k\}=\{x,y,z\}}\hat{\sigma}_i\left[\Pi_i\left(\Pi_j^2 - \Pi_k^2\right)\right] \tag{6}$$

the material spin-splitting, Rashba and Dresselhaus spin-orbit coupling interactions. In the equations above, $\hat{\mathbf{I}}_2$ is the identity matrix of size 2, $\mathbf{r} = (x, y, z)$ is the three-dimensional radius vector,

$$\hat{\mathbf{\Pi}} = -i\hbar\nabla_{\mathbf{r}} + e\mathbf{A}\left(\mathbf{r}\right) \tag{7}$$

is the momentum operator for electrons, $\nabla_{\mathbf{r}}$ stands for the spatial gradient, $\mathbf{A}(\mathbf{r})$ is the vector potential of the magnetic field $\mathbf{B} = \nabla_{\mathbf{r}} \times \mathbf{A}(\mathbf{r})$,

$$\frac{1}{m\left(\mathbf{r},E\right)} = \frac{E_P\left(\mathbf{r}\right)}{3m_0}\left[\frac{2}{\tilde{E}_g\left(\mathbf{r},E\right)} + \frac{1}{\tilde{E}_g\left(\mathbf{r},E\right) + \Delta\left(\mathbf{r}\right)}\right] \tag{8}$$

and

$$g_m(\mathbf{r},E) = 2\left[1 - \frac{1}{m(\mathbf{r},E)}\frac{\Delta(\mathbf{r})}{3\tilde{E}_g(\mathbf{r},E) + 2\Delta(\mathbf{r})}\right] \tag{9}$$

are the electron energy and position dependent electron effective mass and the material Landé factor,

$$\beta(\mathbf{r},E) = \frac{\hbar E_P(\mathbf{r})}{6m_0}\left[\frac{1}{\tilde{E}_g(\mathbf{r},E)} - \frac{1}{\tilde{E}_g(\mathbf{r},E) + \Delta(\mathbf{r})}\right] \tag{10}$$

and

$$\alpha(\mathbf{r},E) = e\frac{\hbar E_P(\mathbf{r})}{6m_0}\left\{\frac{1}{\tilde{E}_g^2(\mathbf{r},E)} - \frac{1}{\left[\tilde{E}_g(\mathbf{r},E) + \Delta(\mathbf{r})\right]^2}\right\} \tag{11}$$

stand for the Rasba spin-orbit coupling parameters [26][37][38], $\gamma(\mathbf{r})$ is the Dresselhaus spin-orbit coupling parameter, $\tilde{E}_g(\mathbf{r},E) = E_g^{\infty} + E - \Delta E_V(\mathbf{r})$ is the effective band gap in the dot (we take the energy reference to $E = 0$ and the energy gap to be E_g^{∞} at the infinity, $\Delta E_V(\mathbf{r})$ is the local valence band offset). The spin-orbit splitting for the valence bands in the system is taken to be $\Delta(\mathbf{r})$, $E_p(\mathbf{r})$ is the Kane interband coupling parameter, $V(\mathbf{r})$ is the actual electronic confinement potential, $\hat{\sigma}$ is the vector of the Pauli matrices, m_0 and e are the free electron mass and elementary charge.

For the quantum dot molecule of undefined symmetry we use a gauge-origin-independent definition for the vector potential (see [31] and references therein): $\mathbf{A}(\mathbf{r}) = \mathbf{B} \times (\mathbf{r} - \bar{\mathbf{r}})/2$, where $\bar{\mathbf{r}}$ stands for the expectation value of the position of the electron in the electron ground state. Using this gauge and Eq. (3) under a weak external magnetic field ($B \to 0$) the spin and magnetic field dependent part of the electron Hamiltonian (after some algebra, keeping only linear in the magnetic field B terms) we can present in the following form [39]:

$$\hat{\mathbf{H}}_{spin} \approx \frac{1}{2}\mu_B \sum_{i,j=x,y,z} \hat{g}_{ij}(\mathbf{r},E)\,\hat{\sigma}_i B_j, \tag{12}$$

where the effective g-factor tensor components are defined as

$$\hat{g}_{ij}(\mathbf{r},E) = g_m(\mathbf{r},E)\,\delta_{ij} + \hat{g}_{R;ij}(\mathbf{r},E) + \hat{g}_{D;ij}(\mathbf{r}), \tag{13}$$

where the Rashba and Dresselhaus couplings bring correspondingly the components $g_{R;ij}$ and $g_{D;ij}$ to the g-tensor:

$$\hat{g}_R(\mathbf{r},E) = -\frac{e}{\mu_B}\begin{pmatrix} \Lambda_y R_y + \Lambda_z R_z & -\Lambda_y R_x & -\Lambda_z R_x \\ -\Lambda_x R_y & \Lambda_x R_x + \Lambda_z R_z & -\Lambda_z R_y \\ -\Lambda_x R_z & -\Lambda_y R_z & \Lambda_x R_x + \Lambda_y R_y \end{pmatrix} \tag{14}$$

and

$$\hat{g}_{D;xx}(\mathbf{r}) = 2\frac{e\hbar^2}{\mu_B}\gamma(\mathbf{r})\left(R_z\nabla_x\nabla_y + R_y\nabla_x\nabla_z\right),$$

$$
\begin{aligned}
\hat{g}_{D;xy}(\mathbf{r}) &= \frac{e\hbar^2}{\mu_B}\gamma(\mathbf{r})\left(-R_z\nabla_y^2 - 2\nabla_z - 2R_x\nabla_x\nabla_z + 2R_z\nabla_z^2\right), \\
\hat{g}_{D;xz}(\mathbf{r}) &= \frac{e\hbar^2}{\mu_B}\gamma(\mathbf{r})\left(-R_y\nabla_z^2 - 2\nabla_y - 2R_x\nabla_x\nabla_y + R_y\nabla_y^2\right), \\
\hat{g}_{D;yx}(\mathbf{r}) &= \frac{e\hbar^2}{\mu_B}\gamma(\mathbf{r})\left(-R_z\nabla_x^2 - 2\nabla_z - 2R_y\nabla_y\nabla_z + R_z\nabla_z^2\right), \\
\hat{g}_{D;yy}(\mathbf{r}) &= 2\frac{e\hbar^2}{\mu_B}\gamma(\mathbf{r})\left(R_x\nabla_y\nabla_z + R_z\nabla_y\nabla_x\right), \\
\hat{g}_{D;yz}(\mathbf{r}) &= \frac{e\hbar^2}{\mu_B}\gamma(\mathbf{r})\left(-R_x\nabla_z^2 - 2\nabla_x - 2R_y\nabla_y\nabla_x + R_x\nabla_x^2\right), \\
\hat{g}_{D;zx}(\mathbf{r}) &= \frac{e\hbar^2}{\mu_B}\gamma(\mathbf{r})\left(-R_y\nabla_x^2 - 2\nabla_y - 2R_z\nabla_z\nabla_y + R_y\nabla_y^2\right), \\
\hat{g}_{D;zy}(\mathbf{r}) &= \frac{e\hbar^2}{\mu_B}\gamma(\mathbf{r})\left(-R_x\nabla_y^2 - 2\nabla_x - 2R_z\nabla_z\nabla_x + R_x\nabla_x^2\right), \\
\hat{g}_{D;zz}(\mathbf{r}) &= 2\frac{e\hbar^2}{\mu_B}\gamma(\mathbf{r})\left(R_y\nabla_z\nabla_x + R_x\nabla_z\nabla_y\right). \qquad (15)
\end{aligned}
$$

In the equations above, the vector $\mathbf{R} = \mathbf{r} - \bar{\mathbf{r}}$ is defined according to the gauge-origin-independent description of the vector potential.

2.2 Mapping of the system parameters

To describe comprehensively all position dependent geometrical and material parameters of the quantum dot molecule we use the mapping procedure for the realistic geometry of the quantum dot molecule on the smooth three dimensional quantum confinement potential [31][32][40]. First, noting that a self-assembled lens-shaped lateral quantum dots are grown starting from a flat substrate parallel to the x-y plane, we model the quantum dot shape profile by a function $h(x, y)$. This function reproduces the local height (along the z direction) at the actual position on the x-y plane for the quantum dot molecule. For lens-shaped circular quantum dots when the distance separating the centers of the dots along the x direction is d (see Fig. 1) we can propose this function as [32]

$$h(x, y) = [h_-(x, y) + h_+(x, y)] \times A(x, y); \qquad (16)$$

where

$$
\begin{gathered}
h_{\mp}(x, y) = \sqrt{R_0^2 - [(x \pm d/2)^2 + y^2]} - R_0 + h_D, \\
when\ \ (x \pm d/2)^2 + y^2 \leq R_B^2;
\end{gathered}
$$

$$
\begin{gathered}
h_{\mp}(x, y) = 0, \\
when\ (x \pm d/2)^2 + y^2 < R_B^2;
\end{gathered}
$$

$$A(x,y) = 1 + d_h \exp\left[-\frac{(x-d/2)^2+y^2}{b^2}\right],$$
$$R_0 = \frac{R_B^2+h_D^2}{2h_D},$$

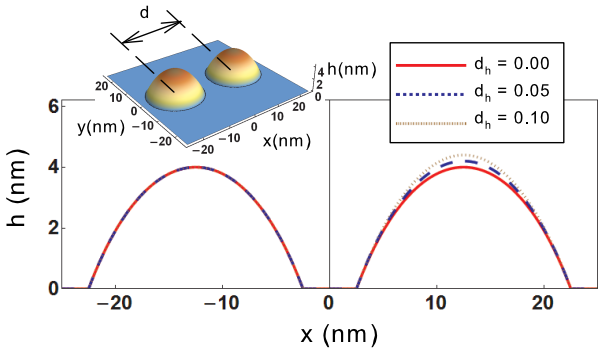

Figure 1: Cross section by the $(x,0,z)$ plane of the lateral quantum dot molecule structure for different values of the parameter d_h ($R_B = 10$ nm, $h_D = 4$ nm, $d = 25$ nm, $d_h = 0.00$). Inset: a three-dimensional view of the molecule.

R_B and h_D are the dots' base radius and maximal height. Possible reflection asymmetry (with respect to reflection in the y-z plane) is described by the function $A(x,y)$, where the range of the reflection asymmetry in the dots' heights is presented by a parameter b. This function allows us to control deviations from the reflection symmetry in the quantum dot molecule shape by a unit-less parameter d_h as [31]

$$d_h = \frac{h(d/2,0)|_{d_h\neq 0} - h(d/2,0)|_{d_h=0}}{h(d/2,0)|_{d_h=0}}, \tag{17}$$

In Fig. 1 we present the actual shape of the quantum dot molecule and its cross section by the $(x,0,z)$ plane for different deviations from the reflection symmetrical configuration. The three-dimensional smooth quantum confinement potential for electrons in the quantum dot molecule $V_e(\mathbf{r})$ can be obtained by the composition- and geometry-dependent profile of the local conduction band offset [31]:

$$V(\mathbf{r}) = \Delta E_{off}\{1 - T_+(s-z)\cdot T_-[z-h(x,y)]\}, \tag{18}$$

where $T_\pm(t) = [1 \pm tanh(t/a)]/2$, ΔE_{off} is the overall conduction band offset between the inner and outer semiconductor materials in the $InAs/GaAs$ heterostructure. The effective substrate-dot interface is assigned to be at the plane $z = s$. The slope and range (the degree of smoothness) of the potential change at the boundaries of the dots are controlled by a parameter a. The three-dimensional confinement potential reflects in a very obvious and natural way the smooth variations of the material parameters across the boundaries of the dots [32][40]. Now we define the unitless mapping function

$$M(\mathbf{r}) = 1 - \frac{V(\mathbf{r})}{\Delta E_{off}}. \tag{19}$$

This function accumulates information about the shape and local material content of the quantum dot molecule. Using the mapping we can reproduce all position dependent material parameters of the structure $D(\mathbf{r})$ (the energy gap $E_g(\mathbf{r})$, the local valence band offset $\Delta E_V(\mathbf{r}) = E_g(\mathbf{r}) - V(\mathbf{r})$, the Kane parameter $E_p(\mathbf{r})$, and the spin-orbit splitting for the valence bands $\Delta(\mathbf{r})$) as the following

$$D(\mathbf{r}) = D^{in} M(\mathbf{r}) + D^{out} [1 - M(\mathbf{r})] . \tag{20}$$

2.3 Simulation strategy

To simulate the g-factor tensor for the ground state of the electron confined in the quantum dot molecule in a weak magnetic field we first solve the non-linear Schrödinger equation with the Hamiltonian presented by Eq. (2) [28][34][37]

$$\left[\hat{\mathbf{p}} \frac{1}{2m(\mathbf{r},E)} \hat{\mathbf{p}} - e\mathbf{F} \cdot \mathbf{r} + V(\mathbf{r}) \right] \Psi_{E_0}(\mathbf{r}) = E_0 \Psi_{E_0}(\mathbf{r}) , \tag{21}$$

where $\hat{\mathbf{p}} = -i\hbar\nabla_{\mathbf{r}}$, $\Psi_{E_0}(\mathbf{r})$ is the ground state wave function. From this solution we obtain the ground state energy E_0 and, consequently, all actual energy- and position-parameters of the system: $m(\mathbf{r}, E_0)$, $g_m(\mathbf{r},E_0)$, $\beta(\mathbf{r},E_0)$, $\alpha(\mathbf{r},E_0)$, and $\mathbf{\Lambda}(\mathbf{r}, E_0)$. The expectation value of a quantity $f(\mathbf{r})$ in the electron ground state with the wave function $\Psi_{E_0}(\mathbf{r})$ is conventionally defined as:

$$\langle f \rangle = \int \Psi^*_{E_0}(\mathbf{r}) f(\mathbf{r}) \Psi_{E_0}(\mathbf{r}) d\mathbf{r}. \tag{22}$$

Therefore, within the linear approximation, we can simulate the expectation values of the electronic position in the quantum molecule $\bar{\mathbf{r}} = \langle \mathbf{r} \rangle$ and all components of the effective g-factor tensor $g_{ij} = \langle \hat{g}_{ij}(\mathbf{r}, E_0) \rangle$.

3 SIMULATION RESULTS AND DISCUSSION

We simulate the electron ground-state energy and wave functions for the lateral quantum dot molecule (Fig. 1) using realistic geometry and material parameters for $InAs/GaAs$ nano-structures [31][41][42][43]. The geometrical characteristics are taken as $R_B = 10$ nm, $h_D = 4$ nm, $b = R_B$, $a = 0.4$ nm, $s = 0.0$ nm. Material parameters we take from [44] and adjust them according to the actual composition and strain inside the dots [14][45]: $E_p^{InAs} = 22.2$ eV, $E_p^{GaAs} = 25.7$ eV, $E_g^{InAs} = 0.842$ eV, $E_g^{GaAs} = 1.52$ eV, $\Delta^{InAs} = 0.38$, $\Delta^{GaAs} = 0.34$ eV. We take 70% of the heterostructure gap difference to be the conductance band offset and 30% to be the valence band offset in the dot. In addition, we correct the value of the material g-factor in the bulk of $GaAs$ including the contribution from the remote bands (see for instance [39] and references therein). The energy and wave functions of the electrons confined in the quantum dot molecule are obtained numerically by the nonlinear iterative method [46] using the COMSOL MULTIPHYSICS package [47]. We

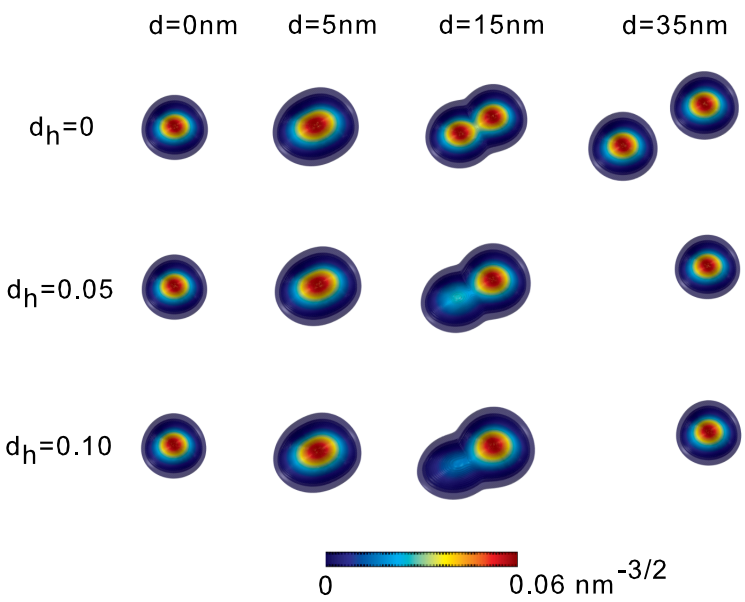

Figure 2: Electron ground state wave function for different d and d_h .

use the wave functions to simulate the expectation values of the electron position and all components of the effective g-factor tensor in the lateral quantum molecule when the distance between dots in the molecule is changing, and when the molecule is reflection symmetrical and when the symmetry is broken.

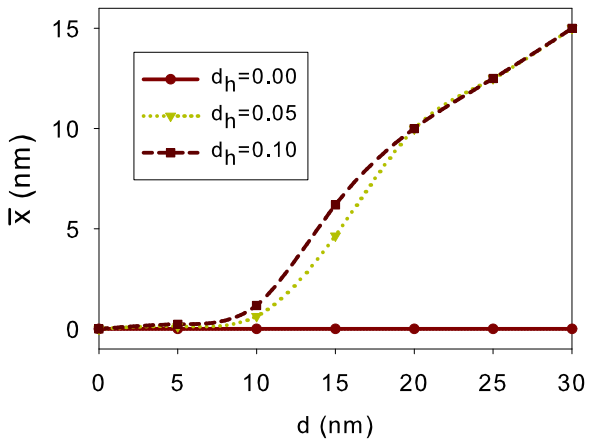

Figure 3: Expectation value of the position of the electron in the ground state on the x-axis for the quantum dot molecules with different geometrical parameters.

First we consider the "static" control of the effective electron g-factor in the lateral quan-

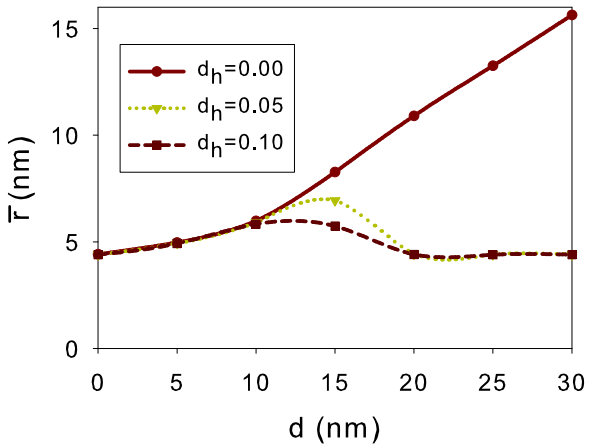

Figure 4: Effective lateral radius of the electron in the quantum dot molecules.

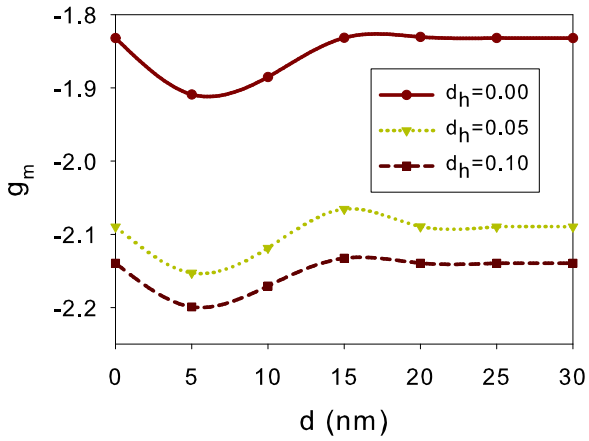

Figure 5: The expectation value of the material Landé factor for different configurations of the system.

tum dot molecule when the system material and geometry is predefined during the structure growth. Fig. 2 presents the ground-state wave function of the electron confined in the quantum dot molecules with different inter-dot distances without external electric fields simulated as it was described above. When the parameter d_h changes from 0 (reflectional symmetrical quantum dot molecule) to 0.1, the wave functions change from a reflectional symmetrical profile (equally distributed within two dots) to reflection non-symmetrical profile (localized in the potential valley of only one dot near $(x = +d/2, y = 0)$ on the x-y plane). For relatively large distances between the dots in the molecule the wave function is localized in one of the potential valleys when the imbalance in the potential profile is really small ($d_h \sim 0.05$). Only when the dots overlap considerably ($d \sim 15$ nm) some relevant distribution of the wave functions between two dots remains up to $d_h \sim 0.1$.

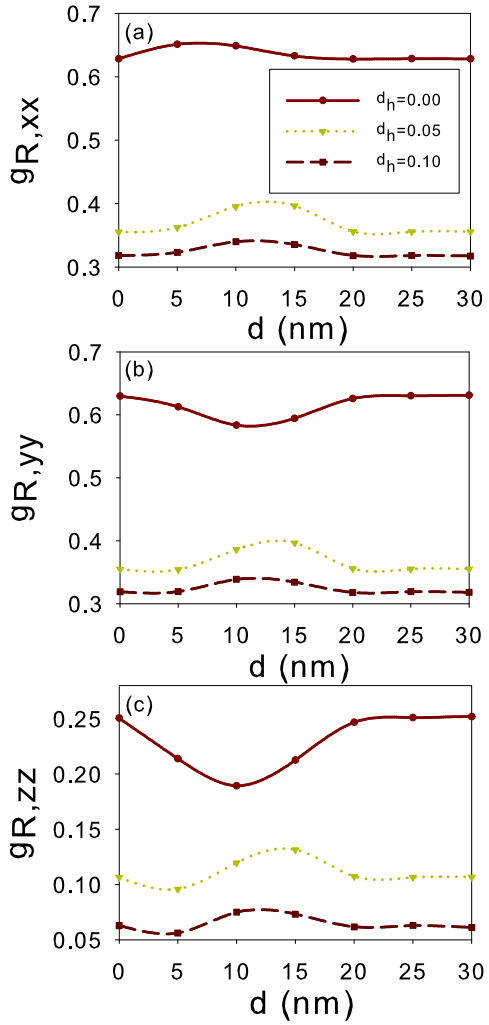

Figure 6: The Rashba coupling part in the expectation values of the diagonal components of the effective g-factor tensor of the quantum dot molecule for different configurations of the system: (a) $g_{R;xx}(d, d_h)$, (b) $g_{R;yy}(d, d_h)$, (c) $g_{R;zz}(d, d_h)$.

Accordingly, as shown in Fig. 3, the expectation value of the electron's position in the ground state (when the parameter d_h increases) rapidly moves from the center of the structure toward the imbalanced potential valley at $(x = +d/2, y = 0)$ on the x-y plane. We note that, for all configurations, the expectation value of the electron position on the y-axis remains unchanged ($\bar{y} = 0$) and on the z-axis only slightly varies near $\bar{z} = 1.8$ nm. From Fig. 4 we see that the effective lateral radius of the electron

$$\bar{r} = \sqrt{\left\langle (\mathbf{r}_\perp - \bar{\mathbf{r}}_\perp)^2 \right\rangle}$$

(where $\bar{\mathbf{r}}_\perp = \langle \mathbf{r}_\perp \rangle$ is the expectation value of the electron position on the x-y plane,

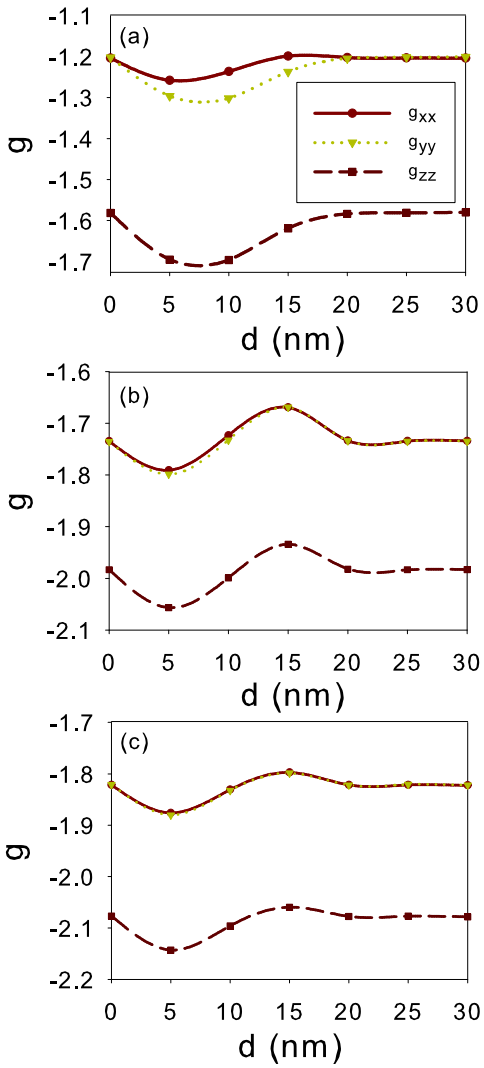

Figure 7: The expectation values of the diagonal components of the effective g-factor for the quantum dot molecule with different configurations: (a) $d_h = 0.00$, (b) $d_h = 0.05$, (c) $d_h = 0.10$.

$\mathbf{r}_\perp = (x, y)$) reflects the $\bar{x}$'s tendency: when the parameter d_h increases the effective lateral radius decreases gradually manifesting the "one potential valley" localization of the electron wave function. The "one valley" localization occurs in the reflection asymmetrical configurations almost immediately (with $d_h \sim 0.01$) as the inter-dot distance reaches 25 nm.

The above-described sensitivity of the electron ground state wave function localization and distribution to the imbalance in the reflection symmetry leads to certain peculiarities in the static control of the effective g-factor. Fig. 5 shows the dependence of the expectation value of the material Landé factor for different configurations of the system. This part

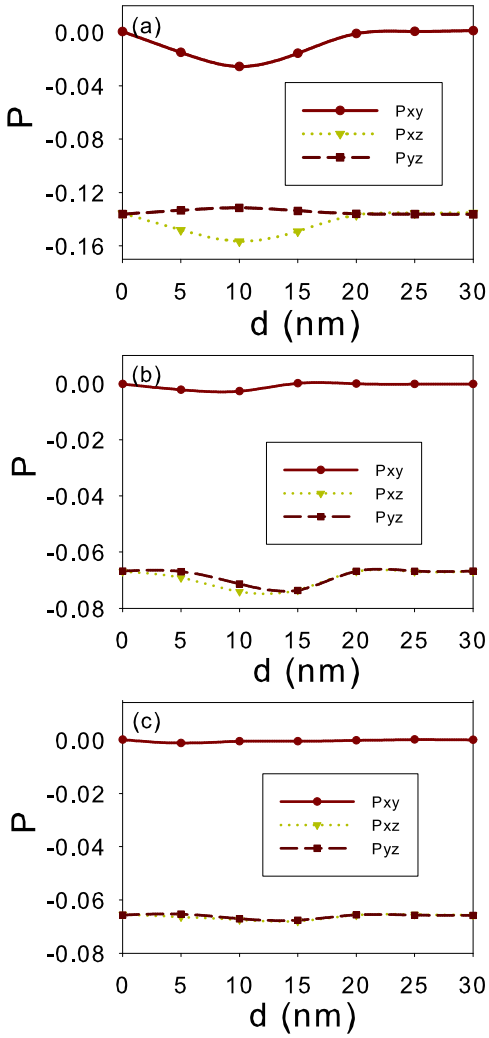

Figure 8: The anisotropy ratio $P_{ij} = (g_{ii} - g_{jj}) / (g_{ii} + g_{jj})$ for the effective g-factor tensor in the systems with different configurations: (a) $d_h = 0.00$, (b) $d_h = 0.05$, (c) $d_h = 0.10$.

of the effective g-factor tensor is obtained in a simple averaging procedure and it clearly reflects the changes in the electron ground wave function distribution in the system. The material average reaches its minimal value when the electron wave function is mainly concentrated inside the dots (the parameters of the strained $InAs$ dominate). The Rashba coupling part in the expectation values of the diagonal components the effective g-factor tensor (see Fig. 6) is generated by the mutual input of the material local parametrs' changes (see Eqs. (5), (10) and (14)) and the wave function actual distribution. It reaches its maximum or minimum according to this interplay. As it can be found from Eqs. (6) and Eq. (15), the Dresselhause coupling plays no role in the diagonal components

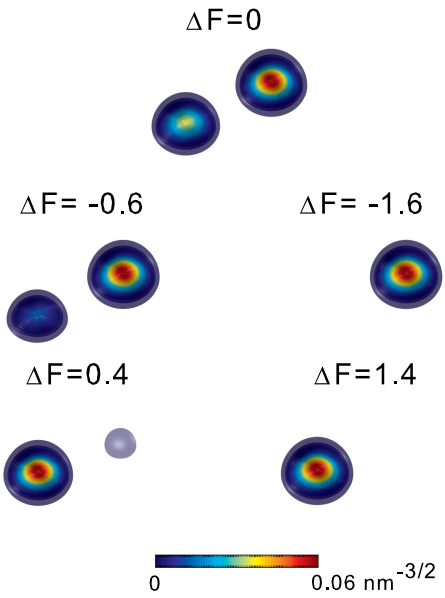

Figure 9: Transformation of the ground state electron wave function of the quantum dot molecule under the external electric field applied along the x direction ($\Delta F = F - F_B$, $d = 35$ nm, $d_h = 0.05$).

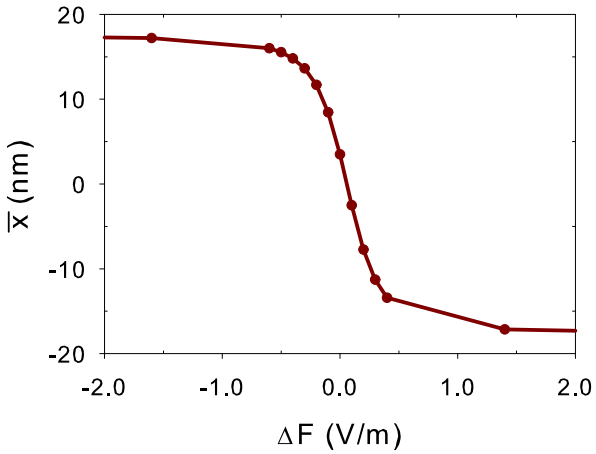

Figure 10: The expectation value of the position of the electron as a function of the external electric field applied along the x direction ($\Delta F = F - F_B$, $d = 35$ nm, $d_h = 0.05$).

of the effective g-factor tensor for the electron in the ground state. At the same time, the off-diagonal components of the the effective g-factor tensor for the electron in the ground states are mainly defined by the Dresselhause coupling. We found them relatively small for the $InAs/GaAs$ lateral quantum dot molecule of the parameters chosen in this work. Therefore, they will be discussed somewhere else.

Fig. 7 presents the expectation values of the diagonal components of the effective g-factor

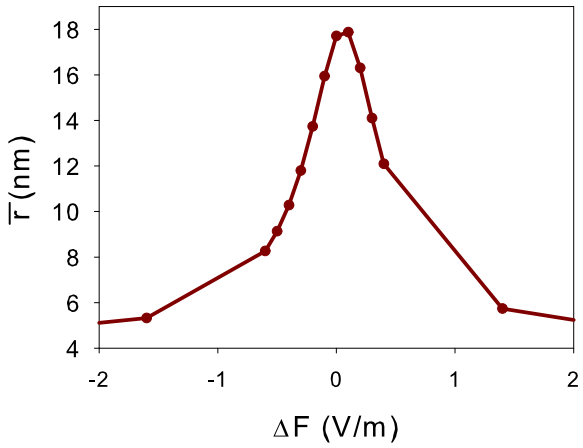

Figure 11: The expectation values of the diagonal components of the effective g-factor for the quantum dot molecule as a function of the external electric field applied along the x direction ($\Delta F = F - F_B$, $d = 35$ nm, $d_h = 0.05$).

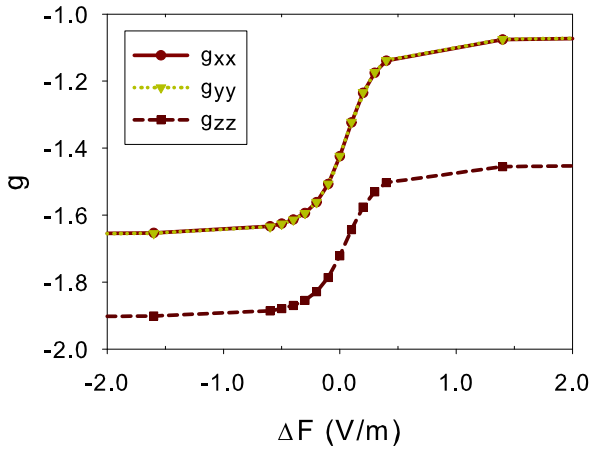

Figure 12: The expectation values of the diagonal components of the effective g-factor as functions of the external electric field applied along the x-direction ($\Delta F = F - F_B$, $d = 35$ nm, $d_h = 0.05$).

including the material and Rashba parts. The dependencies of the diagonal components on the distance and symmetry imbalance in the quantum dot molecule clear represent the interplay in the material the material local parameters' changes (see Eqs. (5) and (10)) and the wave function actual distribution. The general tendencies in the static control (material and structural) of the diagonal components of the effective g-factor tensor for the electron in the ground state is mainly defined by its material part $g_m = \langle \hat{g}_m(\mathbf{r}, E_0) \rangle$. At the same time, the tensor anisotropy is generated completely by the Rashba coupling. In Fig. 8 we show the anisotropy ratio $P_{ij} = (g_{ii} - g_{jj}) / (g_{ii} + g_{jj})$ for the effective g-factor tensor in the system. Clearly, the dependence of the anisotropy ratio on the distance

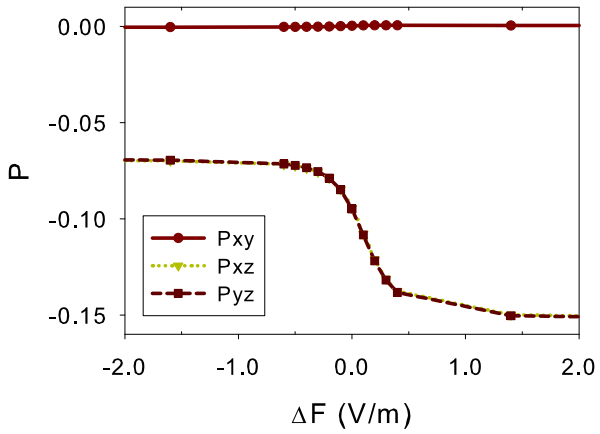

Figure 13: The anisotropy ratio of the effective g-factor as functions of the external electric field applied along the x direction ($\Delta F = F - F_B$, $d = 35$ nm, $d_h = 0.05$).

between two dots is weakening as the asymmetry in the quantum dot molecule increases. This is consistent with the general development of the electron ground state wave function distribution for the asymmetrical molecules (see Fig. 2). We note that actual values of the electron effective g-factor and anisotropy ratio obtained in our simulation are close to those discovered experimentally [48][49][50].

Now we present some results of our simulation of the dynamic control of the electron effective g-factor in the lateral quantum dot molecule when an external electric field is applied to the system. Obviously, this adds more freedom to the operation with the effective g-factor both by the wave function localization and the Rashba coupling changes (see Eqs. (2) and (5)). We have to keep the parameters variations within certain bars. Therefore, in this paper we confine ourselves to the study of the variations of the electron ground state wave function distribution and the effective g-factor in the asymmetrical quantum dot molecule ($d_h = 0.05$) when the dots in the molecule are well separated ($d = 35$ nm). The uniform external electric field $\mathbf{F}$ is applied along the x-axis. Fig. 9 shows how the ground state electron wave function is changed by the external electric field. The electron wave function symmetry can be "recovered" in the quantum molecule when the electric field magnitude is taken to be of about $F_B = 2.021 \times 10^5$ V/m. In Fig. 10 we demonstrate how the expectation value of the electron position can be dynamically controlled near F_B. The wave function symmetry near F_B in this molecule is highly unstable which is in agreement with our previous discussion: a small variation of the field magnitude can push the electron into one or another dot. However, as we demonstrated above, the decrease of the distance between the dots will make the recovered symmetry less sensitive to the field variation. The same consideration we can apply to the effective lateral radius of the electron which dependence on the electric field which is presented in Fig. 11. In Fig. 12 we show a rapid change (actually "switching", "ultimate dynamic control") of the electron effective g-factor, which is a clear result of the wave function

modification and increase of the Rashba coupling (see Eq. (5)) in the asymmetrical quantum dot molecule. We note that the anisotropy ratios P_{xz} and P_{yz} in this system also change rapidly when we vary the electric field near F_B , while P_{xy} remains stable (see Fig. 13). Therefore, we can conclude that the value of the electron effective g-factor and its dynamic upon the external electric field application can provide us with clear and direct information about the electron wave function localization in the lateral quantum dot molecule with broken reflection symmetry.

4 CONCLUSIONS

Using the effective one electronic band energy and position dependent Hamiltonian (incorporating the Rashba and Dresselhaus spin-orbit couplings) and the mapping method, we developed an efficient approach which allows us to simulate the electron effective g-factor in semiconductor nano-objects with complex geometrical shapes and material content. It is clear from our consideration, that the approach allows us to simulate in very cost-efficient manner the electron effective three-dimensional g-factor tensor and analyze an important issue of the static and dynamic control of the tensor components and its anisotropy in semiconductor nano-objects with complex characteristics.
On the base of our approach, in this paper we simulated and characterized (as an example) the components of the the electron effective g-factor tensor and its anisotropy in the lateral semiconductor lateral quantum dot molecules. We obtained the actual value of the electron effective g-factor in the molecule combined from two lens shaped $InAs/GaAs$ quantum dots (which is close to the experimental results) and found that the value relies on the electron wave function localization in the molecule. We investigated the factor dependencies on the distance between the dots, symmetry of the molecule, and external electric field. Our simulation results suggest that the actual value and anisotropy of the effective g-factor tensor are originated from the anisotropy of the actual geometrical and material content in the quantum dot molecule when the Rashba spin-orbit interaction is significant and they can be controlled by a proper engineering of the molecule. In addition, the dynamic control can be performed by the manipulation of the particle wave function localization and the spin-orbit interaction strength by the external electric field. In asymmetrical quantum dot molecules (with small deviations in the dots' heights) the interplay between the static and dynamic controls can lead to a rapid change of the effective g-factor when the external electric field changes. Our approach can be useful for efficient modeling of the magnetic response of semiconductor nano-objects with realistic and non-symmetric geometry under external electric fields.

Acknowledgement

This work is supported by the Ministry of Science and Technology of Taiwan under Contracts No. NSC 102-2112-M-009-003-MY2 and No. MOST-103-2221- E-009-180, and Aiming for the Top University Program of the National Chiao Tung University.

REFERENCES

[1] *Semiconductor nanostructures*, D. Bimberg, ed., Springer, Berlin (2008).

[2] G. Konstantatos and E. H. Sargent, *Nature Nanotechnonogy*, Vol. **5**, pp. 391–400, (2010).

[3] B.C. Lee, O. Voskoboynikov, and C.P. Lee, *Physica E*, Vol. **24**, pp. 87–91, (2004).

[4] J. Chen, W. S. Liao, X. Chen, T. Yang, S. E. Wark, D. H. Son, J. D. Batteas, and P. S. Cremer, *ACS Nano*, Vol. **3**, 173–180, (2009).

[5] S. R. Plissard, D. R. Slapak, M. A. Verheijen, M. Hosevar, G. W. G. Immink, I. van Weperen, S. Nadj-Perge, S. M. Frolov, L. P. Kouwenhoven, and E. P. A. M. Bakkers, *Nano Lett.*, Vol. **12**, pp. 1794–1998, (2012).

[6] *Optics of quantum dots*, G. W. Bryant and G. S. Solomon, eds., Artech House, MA, USA, (2005).

[7] *Biomedical Nanostructures*, K. E. Gonsalves, C. R. Halberstadt, C. T. Laurencin, and L. S. Nair, eds., John Wiley, NJ, USA (2008).

[8] T. Ihn, *Semiconductor Nanostructures*, Oxford University Press, Oxford, (2010).

[9] T. D. Ladd, F. Jelezko, R. Laflamme, Y. Nakamura, C. Monroe, and J. L. O'Brien, *Nature*, Vol. **464**, pp. 45–53, (2010).

[10] J. Fabian, A. Matos-Abiaguea, C. Ertlera, P. Stano, I. Žutić, *Acta Physica Slovaca*, Vol. **57**, pp. 565 – 907, (2007).

[11] D. D. Awschalom and M. E. Flatté, *Nature Physics*, Vol. **3**, pp. 153–159, (2007).

[12] J. Xia, W. Ge, and K. Chang, *Semiconductor Spintronics*, World Scientific Publishing, NJ, USA, (2012).

[13] S. Nadj-Perge, S. M. Frolov, E. P. A. M. Bakkers, and L. P. Kouwenhoven, *Nature*, Vol. **468**, pp. 1084–1087, (2010).

[14] C. E. Pryor and M. E. Flatté, *Phys. Rev. Lett.*, Vol. **96**, pp. 026804-1–026804-4, (2006).

[15] T. P. Mayer Alegre, F. G. G. Hern431ndez, A. L. C. Pereira, and G. Medeiros-Ribeiro, *Phys. Rev. Lett.,* Vol. **97**, pp. 236402-1–236402-4, (2006).

[16] N. A. J. M. Kleemans, J. van Bree, M. Bozkurt, P. J. van Veldhoven, P. A. Nouwens, R. Nötzel, A. Yu. Silov, P. M. Koenraad, and M. E. Flatté, *Phys. Rev. B*, Vol. **79**, pp. 0455311-1–0455311-7, (2009).

[17] G. Medeiros-Ribeiro, M. V. B. Pinheiro, V. L. Pimentel, and E. Marega, *Appl. Phys. Lett.*, Vol. **80**, pp. 4229-4231 , (2002).

[18] A. Schwan, B.-M. Meiners, A. Greilich, D. R. Yakovlev, M. Bayer, A. D. B. Maia, A. A. Quivy, and A. B. Henriques, *Appl. Phys. Lett.*, Vol. **99**, pp. 221914-1–221914-3 (2011).

[19] M. F. Doty, M. Scheibner, I.V. Ponomarev, E. A. Stinaff, A. S. Bracker, V. L. Korenev, T. L. Reinecke, and D. Gammon, *Phys. Rev. Let.*, Vol. **97**, pp. 197202-1–197202-4, (2006).

[20] T. Andlauer and P. Vogl, *Phys. Rev. B*, Vol. **79**, pp. 045307-1–045307-7, (2009).

[21] F.M. Peeters and V.A. Schweigert, *Phys. Rev. B*, Vol. **53**, pp. 1468–1474, (1996).

[22] M. P. Nowak and B. Szafran, *Phys. Rev. B*, Vol. **83**, pp. 035315-1–035315-8, (2011).

[23] S. Prabhakar and R. Melnik, *Jour. Appl. Phys.*, Vol. 108, pp. 064300-1–064300-7, (2010).

[24] Y. Li, J.-L. Liu, O. Voskoboynikov, C.P. Lee, and S.M. Sze, *Comp. Phys. Comm.*, Vol. **140**, pp. 399–404, (2001).

[25] Y. A. Bychkov and E. I. Rashba, *J. Phys. C*, Vol. **17**, pp. 6039–6045 (1984).

[26] Th. Schäpers, G. Engels, J. Lange, Th. Klocke, M. Hollfelder, and H. Lüth, *Jour. Appl. Phys.*, *Vol.* **83**, pp. 4324–4333, (1998).

[27] G. Dresselhaus, *Phys. Rev.*, Vol. **100**, pp. 580–586, (1955).

[28] O. Voskoboynikov, C. P. Lee, and O. Tretyak, *Phys. Rev. B*, Vol. **63**, 165306-1–165306-6, (2001).

[29] C. F. Destefani and S. E. Ulloa, *Phys. Rev. B*, Vol. **71**, pp. 161303-1–161303-6, (2005).

[30] D. Ribeiro-Santos, Fanyao Qu, P. C. Morais, V. Lopez-Richard, and G. E. Marques, *Jour. Appl. Phys.*, Vol. **110**, pp. 124309-1–124309-6, (2011).

[31] O. Voskoboynikov, W. T. Chiu, and L. M. Thu, *Phys. Rev. B*, Vol. **88**, pp. 085310-1–085310-10, (2005).

[32] O. Voskoboynikov, *Ukr. Phys. Jour.*, Vol. **60**, pp. 141–147, (2015).

[33] G. Bastard, *Wave Mechanics Applied to Semiconductor Heterostructures*, Les Edition de Physique, Les Ulis, (1990).

[34] O. Voskoboynikov, Y. Li, H. M. Lu, C. F. Shih, and C. P. Lee, *Phys. Rev. B*, Vol. **66**, pp. 155306-1–155306-6, (2002).

[35] J. I. Climente, J. Planelles, and J. L. Movilla, *Phys. Rev. B*, Vol. **70**, pp. 081301-1–081301-4, (2004).

[36] E. A. de Andrada e Silva, G. C. La Rocca, and F. Bassani, *Phys. Rev.* B, Vol. **50**, pp. 8523-8533, (1994).

[37] H. C. Huang, O. Voskoboynikov, and C. P. Lee, *Phys. Rev. B*, Vol. **67**, pp. 195337-1–195337-8, (2003).

[38] R.Winkler, *Spin-Orbit Coupling Effects in Two-Dimensional Electron and Hole Systems*, Springer, Berlin, (2003).

[39] E. L. Ivchenko, *Optical spectroscopy of Semiconductor Nanostructures*, Alpha Science International Ltd, Harrow, U. K., (2005).

[40] L. M. Thu, W. T. Chiu, and O. Voskoboynikov, *Phys. Rev. B*, Vol. **83**, 125301-1–125301-6, (2011).

[41] O. Voskoboynikov, *Phys. Rev. B*, Vol. **78**, pp. 113310-1–113310-4, (2008).

[42] *Lateral Alignment of Epitaxial Quantum Dots*, C.G. Schmidt, ed., Springer, Berlin, (2007).

[43] R. Nötzel, *IEEE Photon. Jour.*, Vol. **2**, pp. 67–80 (2010).

[44] I. Vurgaman, J.R. Meyer, and L.R. Ram-Mohan, *J. Appl. Phys.*, Vol. **89**, pp. 5815–5870, (2001).

[45] C.E. Pryor and M.-E. Pistol, *Phys. Rev. B*, Vol. **72**, pp. 205311-1–205311,(2005).

[46] Y. Li, O. Voskoboynikov, C.P. Lee, and S.M. Sze, *Comp. Phys. Commun.*, Vol. **141**, pp. 66–72 ,(2001).

[47] http://www.comsol.com

[48] G. Medeiros-Ribeiro, E. Ribeiro, and H. Westfahl Jr., *Appl. Phys. A*, Vol. **77**, pp. 725–729 (2003).

[49] E. Aubry, C. Testelin, F. Bernardot, M. Chamarro, and A. Lemaiître, *App. Phys. Lett.*, Vol. **90**, pp. 242113-1–242113-3, (2007).

[50] A. Schwan, B.-M. Meiners, A. Greilich, D. R. Yakovlev, M. Bayer, A. D. B. Maia, A. A. Quivy, and A. B. Henriques, *App. Phys. Lett.*, Vol. **99**, pp. 221914-1–221914-3, (2011).